Self-propulsive swimmers: Two linked acoustic radiating spheres

M. Rajabi* and A. Hajiahmadi
Sustainable Manufacturing Systems Research Laboratory, School of Mechanical Engineering, Iran University of Science and Technology, Narmak, Tehran, Iran

(Received 14 July 2018; published 10 December 2018)

We propose a simple, practical, and versatile acoustic-driven swimmer, composed of two spherical bodies that may radiate the sound field, monochromatically, at monopole state (breathing mode of vibration) and are linked by a rigid rod. Considering the nonlinear acoustic effects, the net acoustic radiation force exerted on the device is analytically derived and it is shown that the resultant radiation force exerted on the swimmer may be nonzero. Two different configurations are considered: In the first, both spheres radiate, and in the second, one of the spheres is off. In both cases, the full manipulability conditions of swimmers are obtained and the effects of size factors, frequency of radiation, etc., are discussed. Assuming low Reynolds number swimming condition, the frequency-dependent swimming velocity is obtained via the so-called reflection method and the optimal radiating states are discussed. Finally, the challenge of random walk due to host medium fluctuations is discussed and it is shown that the Brownian noise is negligible. Our methodology will open a path toward self-propulsive controllable devices, which may play the role of carriers, machines, or mechanisms at small scales.

DOI: 10.1103/PhysRevE.98.063003

I. INTRODUCTION

Design of artificial small scales (i.e., micro- to molecular-size) swimmers with capability of carrying out intricate targeted tasks such as material, agent, or drug transportation [1] or minimally invasive therapeutic treatments inside the human body [2,3] or sensing, actuating, or cleaning, etc., is challenging due to low Reynolds number operating condition [i.e., assuming usual scales of swimming velocity $\mathrm{v} \sim O(10^0) - O(10^1)\ \mu$m/s, fluid mass density $\rho \sim O(10^3)$ kg/m^3, fluid dynamic viscosity $\eta \sim O(10^{-4})$ Pa s, and length scales $l \sim O(10^0) - O(10^2)\ \mu$m, Reynolds number is obtained as $\Re = \rho v l/\eta \sim O(10^{-5}) - O(10^{-2})$] in which the inertial forces are negligible in comparison with the viscosity effect and noisy fluidic environment in which the steering of the swimmer may be affected by thermal fluctuations or other sources.

Many attempts have been conducted to tackle the issue by introduction of swimmers with motion patterns which break the time reversal symmetry [4–7] or with exploitation of the surface phoretic effects such as electrophoresis, electro-osmosis, diffusiophoresis which may lead to active and passive self-propulsive swimmers [8–16] or by internally or externally induction of thermal field gradients [17,18]. As a different methodology, the passive propulsion mechanism based on asymmetric chemical reaction has been revealed [19–22]. Inspired from the micro-organisms and small-scale living matters motion strategies, artificial swimmers may be designed in which their motion is derived from the wave-like deformation of their main body or their conjugate parts (e.g., flagella or cilia), such as squirmers [23–25], sheets and rods with propagating plane waves along them [4,26,27], elastic filaments [28,29], and nonslender bodies [30–35] with traveling wavelike disturbances, bodies with rotating helix component [6,36,37], or over-twisted elastica [28,38], etc. Another technique which utilizes the oscillation of the host fluid medium to produce self-propulsion of double spherical bodies linked by spring is introduced by Refs. [39,40]. The propulsion based on the acoustic techniques for the case of oscillating entrapped air bubbles is investigated [41,42].

The acoustic radiation force is the result of body-wave interaction. The force is defined as the time-averaged force exerted on body in the way of wave-field propagation, caused by asymmetric pressure induction around the body and the momentum transfer from the host medium to it [43].

The effects associated with the acoustic radiation force is emerged in theory, if someone considers the higher-order terms, at least, up to second-order terms, for field quantities and state equations (e.g., Taylor expansion of acoustic pressure, p, in terms of enthalpy, h, leads to $p = p_0 + (\partial p/\partial h)_{s,0} + (1/2)(\partial^2 p/\partial h^2)_{s,0} h^2 + \text{h.o.t.}$, where p_0 is the pressure at equilibrium condition, h.o.t. stands for higher-order terms, and by setting $(\partial p/\partial h)_{s,0} = \rho_{s,0} = \rho$, which yields $p = -\rho(\partial\psi/\partial t) - (\rho/2)[|\nabla\psi|^2 + (1/2c^2)(\partial\psi/\partial t)^2] + O(\psi^3)$.

Various potential functions associated with the radiation force phenomenon have been introduced in literature especially due to its suitable orders of magnitude with respect to its electromagnetic or optic counterparts, noninvasive nature, in-depth penetration, and steady effect with special applications in biological systems, therapeutic issues and engineering field such as remote noncontact manipulation and drug, agent, or material delivery systems [44–61], trapping [62–67], levitation in microgravity or normal gravity containerless situations [68,69], sorting, classification and collection [70], coagulation [71], fractionation [72,73], bubble clustering [74], cavitation

*majid_rajabi@iust.ac.ir

[75,76], Sonoluminescence [77], transducer calibaration [78], etc.

The present work is based on the fact that if a body could generate an asymmetric acoustic field in the host medium so that the net induced force on the host medium or its body becomes nonzero, the swimming may be achieved as a self-propulsive mechanism. Inspired from the most recent novel idea of self-motile acoustic induced swimmers [79], a new mechanism is offered in the present work which includes two monochromatically acoustic radiating spherical bodies which are connected through a rigid link. Due to the symmetry, the probable swimming direction is along the connecting link. The mechanism has no rigid-body translational or rotational degrees of freedom. Considering this fact that for mechanism with moving parts, the net motion at low Reynolds number condition is achievable if and only if the time reversal symmetry is broken due to a nonreciprocal sequence of translational deformation of the mechanism [4,5] with at least two internal degrees of freedom [5,7], the problem seems challenging. However, the mobility of the proposed device appears nonintuitive due to the fact that in linear acoustic regime, all the field quantities (e.g., pressure and velocity) in the host medium have zero time-averaged (i.e., consider f as field quantity, $\langle f\rangle_t = (1/T)\int_0^T f\,dt$, where $T = 2\pi/\omega$ is the period of acoustic-driven oscillations). We aim to prove the mobility of our proposed mechanism via the concept of acoustic radiation force which is one of the interesting and experimentally observed features associated with nonlinearity effects in wave-body interactions. The acoustic radiation forces exerted on the bodies are analytically calculated and it is shown that the net force on the swimmer may be nonzero. Two distinct configurations are analyzed in numerical results section. The first configuration is composed of two same-sized radiating spheres. In the second configuration, one of the spheres is nonradiating and its size may be different from the radiating one. The second configuration may serve as a single-driver swimmer with a cargo container. In both configurations, our aim is to find the condition for rightward and leftward manipulations and discuss the swimming velocity as an index for performance of the proposed swimmers.

Assuming low Reynolds number swimming condition for typical host media and radiation characteristics of the mechanism in microscales, the swimming velocity is estimated and the functionality of the device is discussed.

II. FORMULATION

The geometry of the problem is depicted in Fig. 1. This figure shows two radiating spheres with radii a_1 and a_2; d is the distance between the center of spheres. Two coordinate systems are used as $\boldsymbol{r}_1 = (x_1, y_1, z_1)$ and $\boldsymbol{r}_2 = (x_2, y_2, z_2)$ placed on the centers of spheres 1 and 2, respectively. The spheres are radiating with the same angular frequency of ω, velocity amplitudes of V_1 and V_2, and phases of γ_1 and γ_2, respectively. The excitation mechanism of the spherical bodies and its probable challenges in practice is not our concern in this work, but the common excitation techniques based on internally implementation of piezoelectric and ceramic actuators is offered in literature [56,80–87].

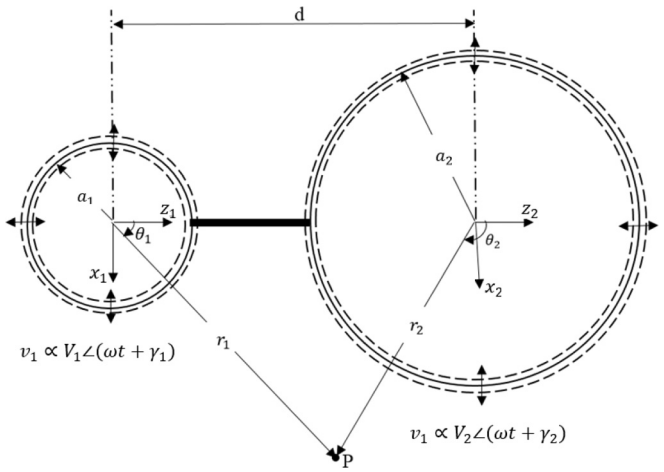

FIG. 1. The geometry of problem: two radiating spheres with radii a_1 and a_2, d is the distance between the center of spheres. Two coordinate systems are used as $\boldsymbol{r}_1 = (x_1, y_1, z_1)$ and $\boldsymbol{r}_2 = (x_2, y_2, z_2)$ placed on the centers of spheres 1 and 2, respectively. The spheres are radiating with the same angular frequency of ω, amplitudes of V_1 and V_2, phases of γ_1 and γ_2, respectively.

A. Acoustic field equations

In linear acoustic regime, the continuity and the Eulerian governing equations for an inviscid and ideal compressible medium that cannot support shear stresses is expressed, respectively, as [88]

$$\frac{\partial \rho}{\partial t} + \rho\,\nabla\cdot\boldsymbol{v} = 0, \tag{1}$$

$$\rho\frac{\partial \boldsymbol{v}}{\partial t} + \nabla p = 0, \tag{2}$$

where ρ denotes the density of fluid host medium in equilibrium state, $\boldsymbol{v}$ is the fluid particles' velocity, and p denotes the ambient pressure. Combination of Eqs. (1) and (2) leads to $\partial^2\boldsymbol{v}/\partial t^2 = c^2\nabla(\nabla\cdot\boldsymbol{v})$, where $c = \{(\partial p/\partial \rho)_{s,0}\}^{1/2}$ is the speed of acoustic waves in fluid host medium, and subscript s,0 means the constant entropy condition due to adiabatic process. Considering the zero vorticity condition of wave propagation phenomenon in linear acoustic (i.e.,$\nabla\times\boldsymbol{v} = 0$), the velocity vector can be expressed as $\boldsymbol{v} = -\nabla\psi$. Substitution of this expression into velocity-time-space equation yields to $\partial^2\psi/\partial t^2 = c^2\nabla^2\psi$.

Considering the monochromatic nature of the wave fields, vibrating with the frequency of ω, the feasible description of the form $\psi(\boldsymbol{r}, t) = \mathrm{Re}(\varphi(\boldsymbol{r})\,e^{-i\omega t})$ leads to the so-called Helmholtz equation as [88]

$$(\nabla^2 + k^2)\varphi = 0, \tag{3}$$

where $k = \omega/c$ is the wave number for the dilatational wave. The solution of the above equation according to the boundary conditions of the system leads to evaluation of the velocity vector field by $\boldsymbol{v} = -\nabla\mathrm{Re}[\varphi(\boldsymbol{r})\,e^{-i\omega t}]$ and the acoustic pressure via $p(r,\theta,\omega) = \rho\partial\mathrm{Re}[\varphi(\boldsymbol{r})\,e^{-i\omega t}]/\partial t$.

It can be easily shown that the expansions of the scalar velocity potential function of outgoing wave from the radiators in spherical coordinate, satisfying the above Helmholtz

equation, have the form [88]

$$\varphi_{\rm rad}^{(\alpha)}(r_\alpha,\theta_\alpha,\omega)=\sum_{n=0}^{\infty}A_n^{(\alpha)}(\omega)h_n(kr_\alpha)P_n(\cos\theta_\alpha),\qquad(4)$$

where $\alpha=1,2$ corresponds to first and second radiator, $A_n^{(\alpha)}(\omega)$ are unknown radiation coefficients, which are to be determined by applying appropriate boundary conditions, h_n is the spherical Hankel function of the first kind, and order n, P_n are Legendre polynomials. Notice that the harmonic time variations throughout the manuscript with $e^{-i\omega t}$ dependence, is suppressed for simplicity. Considering the superposition principle in linear acoustic regime, the total velocity potential is obtained as $\varphi_{\rm tot}^{(\alpha)}=\varphi_{\rm rad}^{(1)}+\varphi_{\rm rad}^{(2)}$.

B. Boundary conditions and translational addition theorem

To determine the unknown coefficients, $A_n^{(\alpha)}(\omega)$, continuity of normal velocity on the surface of spherical bodies is applied as

$$\begin{aligned}\boldsymbol{v}_{\rm tot}^{(1)}\big|_{r_1=a_1}\cdot\hat{e}_r^{(1)}&=\begin{cases}V_1e^{i\gamma_1} & n=0\\ 0 & n>0\end{cases},\\ \boldsymbol{v}_{\rm tot}^{(2)}\big|_{r_2=a_2}\cdot\hat{e}_r^{(2)}&=\begin{cases}V_2e^{i\gamma_2} & n=0\\ 0 & n>0\end{cases},\end{aligned}\qquad(5)$$

where $\hat{e}_r^{(1)}$ and $\hat{e}_r^{(2)}$ are the radial unit vectors on the surface of spheres in (x_1,y_1,z_1) and (x_2,y_2,z_2) coordinate systems. To be able to apply the above boundary conditions, one has to express the velocity potential expansions of Eq. (4) in terms of the other coordinate system variables. This can be done by utilizing translational addition theorem [89].

In this theorem, each term of the velocity potential of coordinate system $\alpha=1,2$ can be expressed in terms of the other coordinate system variables, $\beta=1,2,\alpha\neq\beta$, as

$$\begin{aligned}&h_n(kr_\alpha)P_n(\cos\theta_\alpha)\\&\quad=\sum_{q=0}^{\infty}Q_{0n0q}^{\alpha\beta}(r_{\alpha\beta},\theta_{\alpha\beta})j_q(kr_\beta)P_q(\cos\theta_\beta),\end{aligned}\qquad(6)$$

where

$$\begin{aligned}Q_{0n0q}^{\alpha\beta}(r_{\alpha\beta},\theta_{\alpha\beta})&=(2q+1)i^{q-n}\\&\quad\times\sum_{\sigma=|q-n|}^{q+n}i^\sigma b_\sigma^{n0q0}h_\sigma(kr_{\alpha\beta})P_\sigma(\cos\theta_{\alpha\beta}),\end{aligned}\qquad(7)$$

$$b_\sigma^{n0q\,0}=(2\sigma+1)(nq00|\sigma,0)^2,\qquad(8)$$

in which $(qn00|\sigma,0)$ is the so-called Clebsch-Gordan coefficients [90], $r_{\alpha\beta}=d$ is the distance between the origin of coordinate systems and $\theta_{\alpha\beta}=0,\pi$ is the polar angle between two coordinate systems.

The boundary conditions of Eq. (5) can be rewritten as

$$\begin{aligned}-\frac{\partial\varphi_{\rm tot}^{(1)}}{\partial r_1}\bigg|_{r_1=a_1}&=\begin{cases}V_1e^{i\gamma_1} & n=0\\ 0 & n>0\end{cases},\\ -\frac{\partial\varphi_{\rm tot}^{(2)}}{\partial r_2}\bigg|_{r_2=a_2}&=\begin{cases}V_2e^{i\gamma_2} & n=0\\ 0 & n>0\end{cases},\end{aligned}\qquad(9)$$

which yields

$$\begin{aligned}&A_0^{(1)}h'_0(ka_1)+\sum_{q=0}^{\infty}Q_{0q00}^{21}A_q^{(2)}j'_0(ka_1)=-\tfrac{V_1e^{i\gamma_1}}{k},\\&A_0^{(2)}h'_0(ka_2)+\sum_{q=0}^{\infty}Q_{0q00}^{12}A_q^{(1)}j'_0(ka_2)=-\tfrac{V_2e^{i\gamma_2}}{k},\quad n=0,\\&A_n^{(1)}h'_n(ka_1)+\sum_{q=0}^{\infty}Q_{0q0n}^{21}A_q^{(2)}j'_n(ka_1)=0,\\&A_n^{(2)}h'_n(ka_2)+\sum_{q=0}^{\infty}Q_{0q0n}^{12}A_q^{(1)}j'_n(ka_2)=0,\quad n>0.\end{aligned}\qquad(10)$$

Equations (10) form a linear system of equations with the form of $\mathbf{AX}=\mathbf{B}$, where $\mathbf{X}$ is unknown scattering coefficients $\mathbf{X}=[A_0^{(1)}\ A_1^{(1)}\ \cdots\ A_N^{(1)}\ A_0^{(2)}\ A_1^{(2)}\ \cdots\ A_N^{(2)}]^T$.

C. Acoustic radiation force

For an immersed object with $\boldsymbol{\Upsilon_0}$ as the fixed outer surface at equilibrium condition, interacting with the acoustic monochromatic waves, the emerged acoustic radiation force may be expressed as [91]

$$\langle\boldsymbol{F}\rangle=\int\!\!\int_{\boldsymbol{\Upsilon_0}}\boldsymbol{\Gamma}\cdot d\boldsymbol{\Upsilon},\qquad(11)$$

where $\langle\cdot\rangle$ means time averaged over a period of oscillation, $2\pi/\omega$, $\boldsymbol{\Upsilon_0}$ is the fixed outer surface of the body at equilibrium, $\Gamma_{ij}=-\langle p\rangle\delta_{ij}-\rho p\langle v_iv_j\rangle$ is the Brillouin radiation stress tensor, in which δ_{ij} is Kronecker δ, ρ is the density of host medium, and v_i are the fluid particle velocity components in direct contact with outer surface of the body, $\boldsymbol{\Upsilon}$.

The above formulation of radiation force leads to nonzero values if the Brillouin radiation stress tensor is considered up to at least second order of velocity potential fields (e.g., Taylor expansion of acoustic pressure, p, in terms of enthalpy, h, as $p=p_0+(\partial p/\partial h)_{s,0}+(1/2)(\partial^2p/\partial h^2)_{s,0}h^2+\text{h.o.t.}$, where p_0 is the pressure at equilibrium condition, and by setting $(\partial p/\partial h)_{s,0}=\rho_{s,0}=\rho$ and $(\partial^2p/\partial h^2)_{s,0}=(\partial\rho/\partial h)_{s,0}=(\partial\rho/\partial p)_{s,0}(\partial p/\partial h)_{s,0}=\rho/c^2$, which yields $p=-\rho(\partial\psi/\partial t)-(\rho/2)[|\nabla\psi|^2+(1/2c^2)(\partial\psi/\partial t)^2]+\text{h.o.t.}$). The time-averaged radiation force which is exerted upon radiator α may be written as [91]

$$\begin{aligned}\langle\boldsymbol{f}^{(\alpha)}\rangle&=-\int\!\!\int_S\left(\frac{\rho}{2c^2}\left\langle\left(\frac{\partial\psi^{(\alpha)}}{\partial t}\right)^2\right\rangle\right)\mathbf{n}dS\\&\quad+\int\!\!\int_S\left(\frac{\rho}{2}\langle|\nabla_\alpha\psi^{(\alpha)}|^2\rangle\right)\mathbf{n}dS\\&\quad+\int\!\!\int_S\rho\left\langle\left(v_n^{(\alpha)}\mathbf{n}+v_t^{(\alpha)}\mathbf{t}\right)v_n^{(\alpha)}\right\rangle dS,\end{aligned}\qquad(12)$$

where S is equilibrium position of the radiator's surface,

$$\psi^{(\alpha)}=\mathrm{Re}\left(\varphi_{\rm tot}^{(\alpha)}\right)=\sum_{n=0}^{\infty}R_n^{(\alpha)}P_n(\cos\theta_\alpha),\qquad(13)$$

where $R_n^{(\alpha)} = \mathrm{Re}[(U_n^{(\alpha)} + iV_n^{(\alpha)})e^{-i\omega t}]$, in which $U_n^{(\alpha)} = (\chi_n^{(\alpha)} + \xi_n^{(\alpha)})j_n(kr_\alpha) - \lambda_n^{(\alpha)} y_n(kr_\alpha)$ and $V_n^{(\alpha)} = (\lambda_n^{(\alpha)} + \varsigma_n^{(\alpha)})j_n(kr_\alpha) + \chi_n^{(\alpha)} y_n(kr_\alpha)$. By defining $\chi_n^{(\alpha)} = \mathrm{Re}(A_n^{(\alpha)})$, $\lambda_n^{(\alpha)} = \mathrm{Im}(A_n^{(\alpha)})$, $\xi_n^{(\alpha)} = \mathrm{Re}(\sum_{q=0}^{\infty} Q_{0q0n}^{\beta\alpha} A_q^{(\beta)})$, $\varsigma_n^{(\alpha)} = \mathrm{Im}(\sum_{q=0}^{\infty} Q_{0q0n}^{\beta\alpha} A_q^{(\beta)})$,

$\alpha, \beta = 1, 2$, while $\alpha \neq \beta$, the radiation force with respect to z axis, $\langle \boldsymbol{f}^{(\alpha)} \rangle = \langle f_z^{(\alpha)} \rangle \hat{e}_z$, can be rewritten as

$$\langle f_z^{(\alpha)} \rangle = \langle f_r^{(\alpha)} \rangle + \langle f_\theta^{(\alpha)} \rangle + \langle f_{r\theta}^{(\alpha)} \rangle + \langle f_t^{(\alpha)} \rangle, \tag{14}$$

where

$$\langle f_r^{(\alpha)} \rangle = -\pi a_\alpha^2 \rho \int_0^\pi \left\langle \left(\frac{\partial \psi^{(\alpha)}}{\partial r_\alpha} \right)^2 \Big|_{r_\alpha = a_\alpha} \right\rangle \sin\theta \cos\theta d\theta = -2\pi (ka_\alpha)^2 \rho \sum_{n=0}^{\infty} \frac{2(n+1)}{(2n+1)(2n+3)} \langle R_n^{'(\alpha)} R_{n+1}^{'(\alpha)} \rangle,$$

$$\langle f_\theta^{(\alpha)} \rangle = \pi \rho \int_0^\pi \left\langle \left(\frac{\partial \psi^{(\alpha)}}{\partial \theta_\alpha} \right)^2 \Big|_{r_\alpha = a_\alpha} \right\rangle \sin\theta \cos\theta d\theta = 2\pi \rho \sum_{n=0}^{\infty} \frac{2n(n+1)(n+2)}{(2n+1)(2n+3)} \langle R_n^{(\alpha)} R_{n+1}^{(\alpha)} \rangle,$$

$$\begin{aligned} \langle f_{r\theta}^{(\alpha)} \rangle &= 2\pi a_\alpha \rho \int_0^\pi \left\langle \left(\frac{\partial \psi^{(\alpha)}}{\partial r_\alpha} \right)\Big|_{r_\alpha = a_\alpha} \left(\frac{\partial \psi^{(\alpha)}}{\partial \theta_\alpha} \right)\Big|_{r_\alpha = a_\alpha} \right\rangle \sin^2\theta d\theta \\ &= 2\pi k a_\alpha \rho \sum_{n=0}^{\infty} \left[\frac{2n(n+1)}{(2n+1)(2n+3)} \langle R_n^{(\alpha)} R_{n+1}^{'(\alpha)} \rangle - \frac{2(n+1)(n+2)}{(2n+1)(2n+3)} \langle R_n^{'(\alpha)} R_{n+1}^{(\alpha)} \rangle \right], \end{aligned}$$

$$\langle f_t^{(\alpha)} \rangle = -\frac{\pi {a_\alpha}^2 \rho}{c^2} \int_0^\pi \left\langle \left(\frac{\partial \psi^{(\alpha)}}{\partial t} \right)^2 \Big|_{r_\alpha = a_\alpha} \right\rangle \sin\theta \cos\theta d\theta = -2\pi \rho (ka_\alpha)^2 \sum_{n=0}^{\infty} \frac{2(n+1)}{(2n+1)(2n+3)} \langle R_n^{(\alpha)} R_{n+1}^{(\alpha)} \rangle, \tag{15}$$

in which $\langle R_n^{'(\alpha)} R_{n+1}^{'(\alpha)} \rangle = (U_n' U_{n+1}' + V_n' V_{n+1}')/2$, $\langle R_n^{(\alpha)} R_{n+1}^{(\alpha)} \rangle = (U_n U_{n+1} + V_n V_{n+1})/2$, $\langle R_n^{(\alpha)} R_{n+1}^{'(\alpha)} \rangle = (U_n U_{n+1}' + V_n V_{n+1}')/2$ and $\langle R_n^{'(\alpha)} R_{n+1}^{(\alpha)} \rangle = (U_n' U_{n+1} + V_n' V_{n+1})/2$.

D. Stokes flow and swimming velocity

For low Reynolds number swimming of micro- or millimeter-sized particles, the governing equations considering the Stokes flow and incompressibility condition, can be written as [92]

$$\mu \nabla^2 \boldsymbol{v} = \nabla p + \boldsymbol{f}, \tag{16}$$

$$\nabla \cdot \boldsymbol{v} = 0, \tag{17}$$

where μ is the viscosity of fluidic environment, $\boldsymbol{v}$ is the flow velocity field, p is the pressure field and $\boldsymbol{f}$ is the density of external body forces on the fluid which is neglected in our analysis. Considering the unknown swimming velocity of the proposed swimmer as, $\boldsymbol{V}_s = V_s \hat{e}_z$, where $\hat{e}_z$ is the common unit vector in z_1 or z_2 directions, and assuming the no-slip boundary conditions on the spherical bodies, $\boldsymbol{v} = V_s \hat{e}_z$ at $\boldsymbol{r}_1 = a_1 \hat{e}_r^{(1)}$ and $\boldsymbol{r}_2 = a_2 \hat{e}_r^{(2)}$, along with the zero-velocity boundary condition at infinity, $\boldsymbol{v} \to 0$ at $\boldsymbol{r}_1, \boldsymbol{r}_2 \to \infty$, the obtained boundary value problem has been solved by reflections method [93]. Due to the linearity of governing equations and boundary conditions, which leads to the relation between the required external applied propulsion force on the spheres, F_i, $i = 1, 2$, and the swimming velocity, V_s, up to $O(a_1^{p_1} a_2^{p_2}/d^5)$, $p_1 + p_2 = 5$ as

$$\begin{aligned} F_i = 6\pi \mu a_1 V_s \Bigg[& 1 - \frac{3}{2}\frac{a_2}{d} + \frac{9}{4}\frac{a_1 a_2}{d^2} + \frac{1}{2}\left(\frac{a_1^2 a_2}{d^3} - \frac{27}{4}\frac{a_1 a_2^2}{d^3} + \frac{a_2^3}{d^3} \right) \\ & + \frac{3}{4}\left(-2\frac{a_1^3 a_2}{d^4} + \frac{27}{4}\frac{a_1^2 a_2^2}{d^4} + \frac{3 a_1 a_2^3}{d^4} \right) - \frac{9}{4}\left(\frac{a_1^3 a_2^2}{d^5} + \frac{27}{8}\frac{a_1^2 a_2^3}{d^5} + \frac{a_1 a_2^4}{d^5} \right) \Bigg]. \end{aligned} \tag{18}$$

Considering $F_1 = f_z^{(1)} + T$ and $F_2 = f_z^{(2)} - T$, where $f_z^{(1)}$ and $f_z^{(2)}$ are acoustic radiation forces on spheres 1 and 2, respectively, and T as the rigid link force, we obtain $F_1 = F_2 = (f_z^{(1)} + f_z^{(2)})/2$, which leads to the swimming velocity up

to first, third and fifth order of aspect ratio, $O(a_1^{p_1}a_2^{p_2}/d^5)$, as

$$V_s = \frac{\left(f_z^{(1)} + f_z^{(2)}\right)}{12\pi\mu a_1} \begin{cases} \left(1 - \frac{3}{2}\frac{a_2}{d}\right)^{-1}, & \text{first order} \\ \left(1 - \frac{3}{2}\frac{a_2}{d} + \frac{9}{4}\frac{a_1 a_2}{d^2} + \frac{1}{2}\left(\frac{a_1^2 a_2}{d^3} - \frac{27}{4}\frac{a_1 a_2^2}{d^3} + \frac{a_2^3}{d^3}\right)\right)^{-1}, & \text{third order} \\ \left(1 - \frac{3}{2}\frac{a_2}{d} + \frac{9}{4}\frac{a_1 a_2}{d^2} + \frac{1}{2}\left(\frac{a_1^2 a_2}{d^3} - \frac{27}{4}\frac{a_1 a_2^2}{d^3} + \frac{a_2^3}{d^3}\right)\right. & \\ \left. + \frac{3}{4}\left(-2\frac{a_1^3 a_2}{d^4} + \frac{27}{4}\frac{a_1^2 a_2^2}{d^4} + \frac{3a_1 a_2^3}{d^4}\right) - \frac{9}{4}\left(\frac{a_1^3 a_2^2}{d^5} + \frac{27}{8}\frac{a_1^2 a_2^3}{d^5} + \frac{a_1 a_2^4}{d^5}\right)\right)^{-1}. & \text{fifth order} \end{cases} \tag{19}$$

It should be noted that the obtained swimming velocity, is the time-averaged value considering the nature of driving acoustic radiation force [55,56,94–96].

Also, the steady Stokes condition is assumed in which the inertial, buoyant, history, and other contributing terms are neglected for simplicity [43,97], first due to this fact that at low Reynolds number hydrodynamics, the viscous drag force dominancy is a practical assumption, and second, the main aim of the present work is just to show the functionality of the proposed acoustic-driven swimmer rather than accurate modeling of the swimmer dynamics and the hydrodynamics of the host medium.

III. RESULTS AND DISCUSSIONS

In this section, we consider a numerical example to study the general behavior and performance of the proposed swimmer. Two distinct configurations are considered:

(1) In the first one, two spherical bodies radiate and for simplicity, the geometrical configuration is limited to $a_1 = a_2 = a$. In this case, we aim to give the feasibility study and investigate the influence of the design parameters such as the frequency of operation, phase difference and the aspect ratio on the swimming velocity.

(2) In the second one, the body 2 does not radiate and may have larger radius than the sphere 1. This configuration may be considered as a self-propulsive carrier with a cargo container. The radiating sphere plays the role of driving motor of the system. The proposed configuration overcomes the safety and compatibility problems associate with the probable effects of radiating driver mechanism (e.g., piezoelectric actuators) on the carried material, drug, or agent in the container. In this case, the complete manipulability (i.e., rightward and leftward motion) would be the challenging factor.

In both cases, $a_1 = 100\,\mu$m and the velocity of radiation is set as $V = P_0^2/(\rho c)$ where P_0 is the an index of maximum induced pressure in the medium, $P_0 = 10^4$ Pa. The fluid medium is assumed to be water in atmospheric condition, density $\rho = 10^3\,\text{kg/m}^3$, speed of sound waves $c = 1480\,\text{m/s}$, and viscosity $\eta = 8.9 \times 10^{-4}\,\text{Pa s}$.

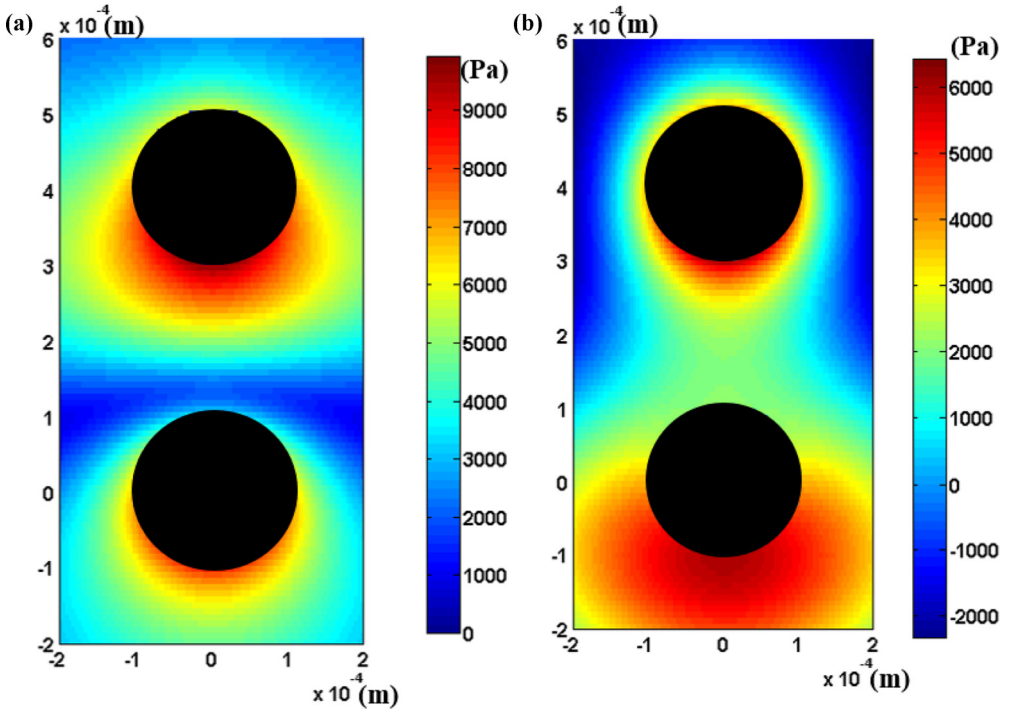

FIG. 2. (a) Two-dimensional (2D) plot of amplitude and (b) real of acoustic pressure contour in xz plane, respectively, for the case of $d/a = 4$ and $\Delta\Phi = \gamma_1 - \gamma_2 = \pi/2$.

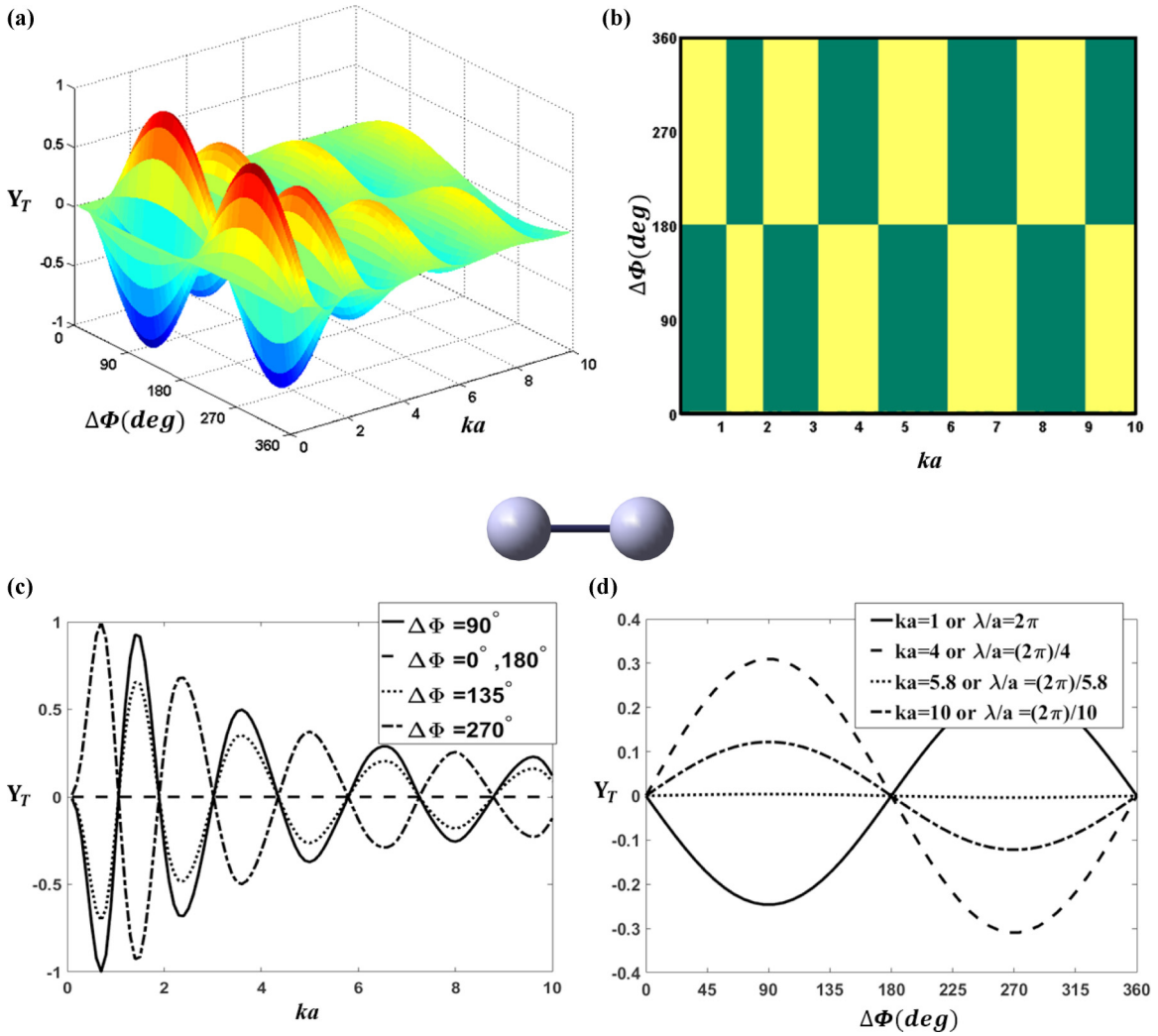

FIG. 3. (a) Three-dimensional (3D) plot of normalized radiation force function, Y_T, as a function of nondimensional frequency, $0 < ka < 10$, and phase difference, $0 \leqslant \Delta\Phi = \gamma_1 - \gamma_2 \leqslant 2\pi$. (b) The top-view of 3D plot of Y_T to illustrate the locus of zero driving force states and the positive [rightward motion along $(z+)$ direction] and negative [leftward motion along $(z-)$ direction], yellow- and green-colored rectangular regions in $ka, \Delta\Phi-$ plane, respectively. (c) Some selected slices of 3D plot of Y_T for phase differences, $\Delta\Phi = 0^\circ, 90^\circ, 180^\circ, 180, 270^\circ$. (d) Some selected slices of 3D plot of Y_T for nondimensional frequencies, $ka = 1.0, 4.0, 5.8, 10.0$ (i.e., $\lambda/a = 2\pi, (2\pi)/4, (2\pi)/5.8, (2\pi)/10$). (Configuration 1.)

The validity of the computations is verified by first: Considering the limiting case of $d/a \to \infty$ with existence of progressive plane wave in z direction, the radiation force function of body 1 is computed as a function of nondimensional frequency, ka, and Fig. 3 of Ref. [91] is obtained; second, by setting $d/a = 5$, $V_1 = V_2 = 0$ and adding the effect of a plane progressive monochromatic incident field to Eq. (11) and calculating the scattering cross section function, as a function of nondimensional frequency, ka, Fig. 3 of Ref. [98] is obtained.

Figures 2 through 8 belong to the case of configuration 1 and Figs. 8 through 10 discuss the case of configuration 2. To show the emergence of asymmetric acoustic pressure distribution in the case of out-of-phase radiation, Figs. 2(a) and 2(b) illustrate 2D amplitude and real (captured at time $t = 0$) of acoustic pressure contour in xz plane, respectively, for the case of $d/a = 4$ and $\Delta\Phi = \gamma_1 - \gamma_2 = \pi/2$.

For normalizing the radiation force amplitude, $f_z^{(\alpha)}$, the normalized radiation force is defined as $\bar{f}^{(\alpha)} = f_z^{(\alpha)}/(P_r\, S_c)$ where $S_c = \pi a_1^2$ denotes the cross sectional area of spherical bodies, $P_r = \rho\, V^2/2$ is an index of radiated pressure and $\bar{f}^{(\alpha)}$ is the nondimensional radiation force. The normalized time-averaged total radiation forces on the swimmer is denoted as $Y_T = \bar{f}^{(1)} + \bar{f}^{(2)}$, which play the role of driver in Eq. (19).

Figure 3(a) illustrates the 3D plot of total normalized radiation force, Y_T, as a function of nondimensional frequency, $0 < ka < 10$, and phase difference, $0 \leqslant \Delta\Phi = \gamma_1 - \gamma_2 \leqslant 2\pi$. Figure 3(b) shows the top-view of Fig. 3(a) to illustrate the locus of zero driving force states and the positive (rightward motion) and negative (leftward motion) values of force, which are depicted as yellow and green colored rectangular regions in $(ka, \Delta\Phi)$ plane, respectively. The zero driving force state occurs for $\Delta\Phi = 0^\circ, 180^\circ$, independent of frequency of operation. Moreover, it is seen that for specified

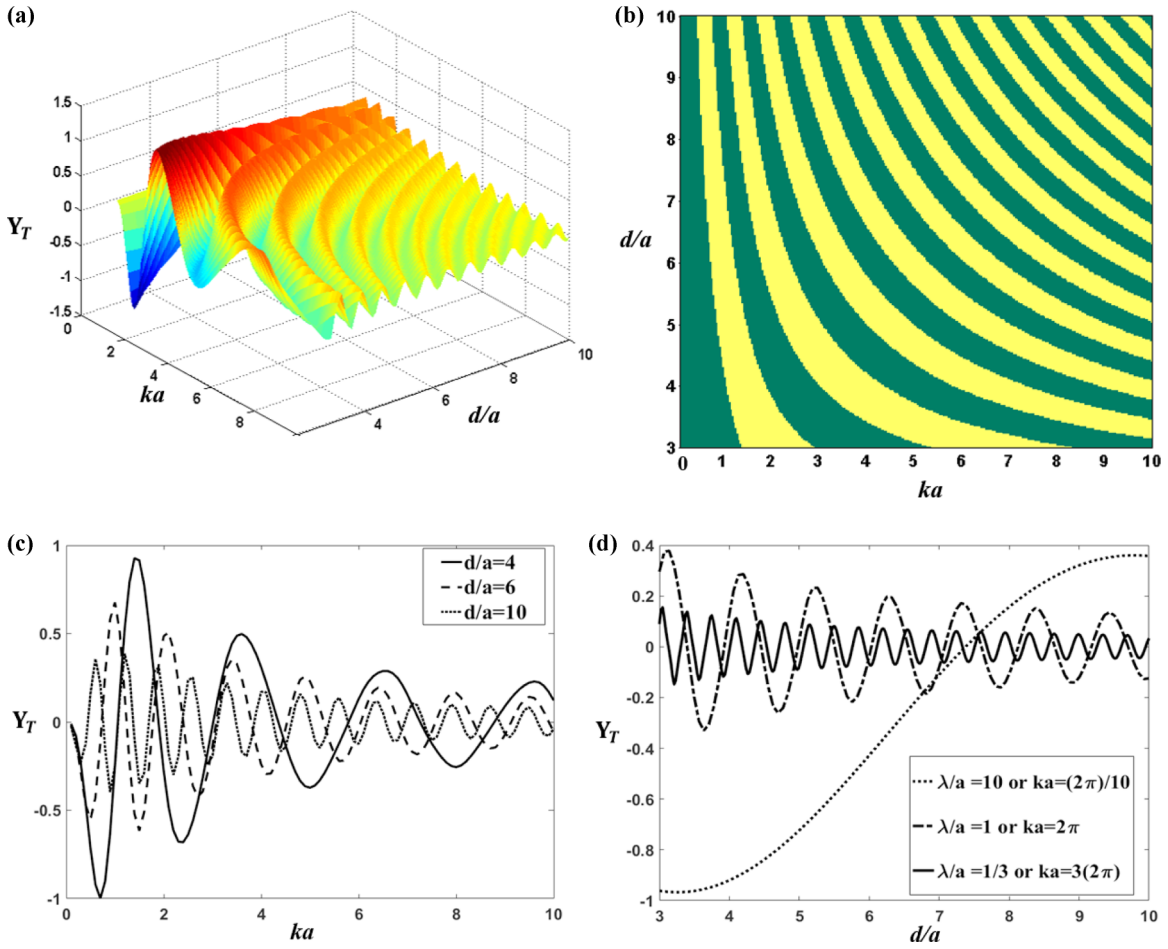

FIG. 4. (a) Three-dimensional (3D) plot of normalized radiation force function, Y_T, as a function of nondimensional frequency, $0 < ka < 10$, and geometrical aspect ratio, $3 < d/a < 10$, for $\Delta\Phi = 90^\circ$ corresponding to the maximum swimming state. (b) The top-view of three-dimensional (3D) plot of Y_T to illustrate the locus of zero driving force states and the positive (rightward motion) and negative (leftward motion), yellow and green colored regions in $ka, d/a-$ plane, respectively. (c) Some selected slices of 3D plot of Y_T for selected aspect ratios, $d/a = 4,\ 6,\ 10$. (d) Some selected slices of 3D plot of Y_T for three categories of wavelength to radius of spheres ratios as $\lambda/a = 10,\ 1,\ 1/3$ [i.e., $ka = (2\pi)/10,\ 2\pi,\ 3(2\pi)$] corresponding to low, medium, and high wavelength to size ratios. (Configuration 1.)

frequencies, zero driving force states emerge independent of phase difference of spheres. It can be easily shown that for any specified fluid medium, the frequencies of zero-driving force states are dependent to geometrical aspect ratio of swimmer, d/a. The existence of these zero-state frequencies (i.e., they can be exactly found from the simultaneous solution of $\partial Y_T/\partial(\Delta\Phi) = 0$ and $Y_T = 0$) is not obvious and it cannot be inferred from force equations. It seems the physical interpretation especially the switching nature of the force states, needs further in-depth investigation into pressure and momentum distribution balance on the radiating bodies at specified wavelength to size ratios.

Figure 3(c) shows some selected slices of Fig. 3(a) for phase differences, $\Delta\Phi = 0^\circ,\ 90^\circ,\ 180^\circ,\ 270^\circ$. It is seen that the total driving force has oscillatory behavior with respect frequency of operation. As the frequency increases, the total driving force decreases. The oscillatory behavior leads to positive and negative values of driving force which means rightward (along z direction) and leftward motion. An interesting event is the zero-driving force states which occur for all values of phase differences, at the same frequencies.

The variation of driving force with respect to phase difference for selected nondimensional frequencies, $ka = 1.0,\ 4.0,\ 5.8,\ 10.0$ [i.e., $\lambda/a = 2\pi,\ (2\pi)/4,\ (2\pi)/5.8,\ (2\pi)/10$], is shown in Fig. 3(d). The selected nondimensional frequency of $ka = 5.8$ is corresponding to zero driving force state. It is seen that the extremes (maximum amplitude) of driving force at any specified frequency, occurs at $\Delta\Phi = 90^\circ$ and $\Delta\Phi = 270^\circ$. At any specified frequency of operation, a phase switch of $\Delta\gamma_1 = \pm 180^\circ$ or $\Delta\gamma_2 = \pm 180^\circ$, leads to direction switch of swimming. It is important to note that at any specified frequency, the phase difference between the spheres may play the role of speed controller from zero to the frequency-dependent maximum value.

Figure 4(a) illustrates the 3D plot of total normalized radiation force, Y_T, as a function of nondimensional frequency, $0 < ka < 10$, and geometrical aspect ratio, $3 < d/a < 10$. It should be noted that as d/a closes to 2, the error of reflection method for obtaining swimming velocity increases. Therefore, we confine our numerical results to minimum of $d/a = 3$. The phase difference is set $\Delta\Phi = 90^\circ$, corresponding to the maximum swimming state. The variation of

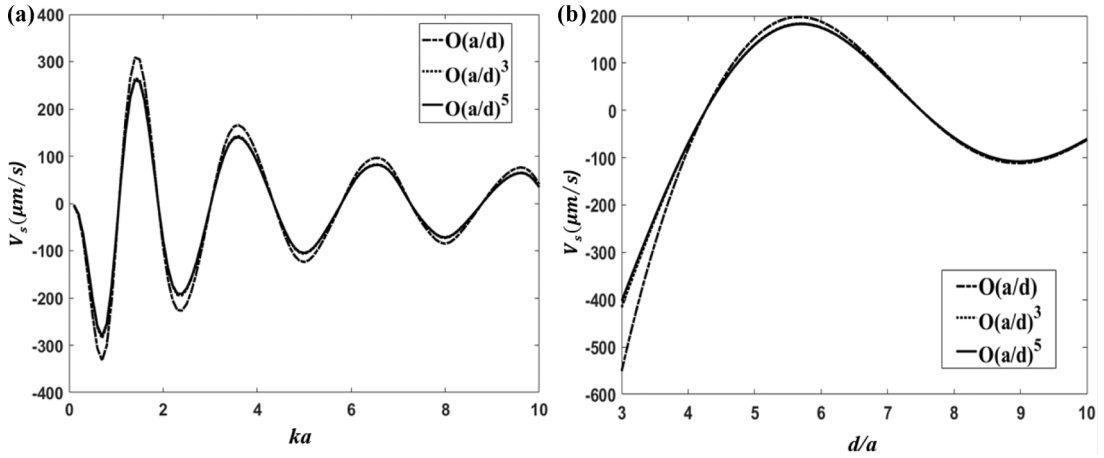

FIG. 5. (a) The variation of swimming velocity, V_s, in its maximum state, $\Delta\Phi = 90^\circ$, with respect to normalized frequency, ka, at constant aspect ratio, $d/a = 4$ and (b) The variation of swimming velocity, V_s, in its maximum state, $\Delta\Phi = 90^\circ$, with respect to aspect ratio, d/a, at constant nondimensional frequency, $ka = 1$, for three cases of approximation order obtained from the reflection method, up to first, third and fifth order of aspect ratio index, $O(a_1^{p_1} a_2^{p_2}/d^{p_1+p_2})$. (Configuration 1.)

driving force illustrates oscillatory behavior and decreasing trend with respect to both frequency and aspect ratio. Figure 4(b) shows the top-view of Fig. 4(a) to illustrate the locus of zero driving force states and the positive (rightward motion) and negative (leftward motion), yellow and green colored rectangular regions in ka, d/a plane, respectively.

Figure 4(c) shows some selected slices of Fig. 4(a) for selected aspect ratios, $d/a = 4,\ 6,\ 10$. Figure 4(d) illustrates some slices of Fig. 4(a) for three categories of wavelength to radius of spheres ratios as $\lambda/a = 10,\ 1,\ 1/3$ [i.e., $ka = (2\pi)/10,\ 2\pi,\ 3(2\pi)$] corresponding to low, medium, and high wavelength to size ratios. From the design point of view, as the frequency and aspect ratio increases, the amplitude of driving force decreases. Considering the maximum amplitude of normalized driving force as $\mathrm{Y}_T \sim 1$, which occurs at $\lambda/a \sim 9.1$ (i.e., the exact value of normalized frequency of maximum state is $ka \sim 0.69$), it is found that the maximum order of possible driving force is estimated as $O(\pi\rho a^2 V^2/2)$. For the given numerical example, $a \sim 10^2\,\mu$m, $V \sim 10^{-3}$ m/s, the order of maximum driving force is $\sim 10^{-10}\,N$, occurs at the frequency of operation, $\sim 10^6$ Hz. The given radiating sphere's velocity is equivalent to the amplitude of radiation of the bodies, $\sim O(V/\omega) \sim 10^{-1}\,\mu$m. Comparing the obtained order of magnitude of the driving force which seems small, with the fluctuation noise amplitude due to thermal induced random fluctuations associated with the atoms of host medium [4,5,99], $(6\pi\eta a k_B T)^{1/2} \sim O(10^{-13})\,N$ where $k_B \approx 1.38 \times 10^{-23}(\mathrm{kg\,m^2})/(s^2\mathrm{K})$ is Boltzmann constant of host medium and $T \sim O(10^2)\,\mathrm{K}$ is temperature of ambient medium, the effect of Brownian motion or random walk is negligible.

In addition, following the estimation of Refs. [100–104], for acoustic viscous boundary layer thickness, δ, as $\sim O([\eta/(\rho\omega)])^{1/2}) \sim O(10^{-1})\,\mu$m, and considering the situation of $\delta/a \ll 1$, we can disregard the effects of acoustic streaming.

In following, our interest is to study the swimming velocity which may be considered as an index of the performance of the proposed self-propulsive device. Considering the used reflection method, we aim to examine the convergence of the method which is related to the aspect ratio, d/a. Figure 5(a) shows the variation of swimming velocity, V_s, in its maximum state, $\Delta\Phi = 90^\circ$, with respect to normalized frequency, ka, at constant aspect ratio, $d/a = 4$ and Fig. 5(b) shows the variation of swimming velocity, V_s, in its maximum state, $\Delta\Phi = 90^\circ$, with respect to aspect ratio, d/a, at constant nondimensional frequency, $ka = 1$, for three cases of approximation up to first, third and fifth order of aspect ratio index, $O(a_1^{p_1} a_2^{p_2}/d^{p_1+p_2})$, in Eq. (19). As it is clear, the error between the three orders of approximations decreases as the frequency and aspect ratio increases, while the errors between the first order approximation and fifth one, at the worst case in the given example (i.e., aspect ratio of $d/a = 3$ and the nondimensional frequency of $ka \approx 0.7$) reports the errors up to 30% . Moreover, the errors is in its maximum states which occurs at the extremes of swimming velocity function. From the given comparison, it may be concluded that the approximation up to at least third order is necessary.

Figures 6(a)–6(c) repeat Figs. 4(a), 4(c), and 4(d), respectively, for swimming velocity, V_s.The phase difference is set, $\Delta\Phi = 90^\circ$, to focus on the maximum swimming velocity state. The general pattern of variations with respect to frequency and aspect ratio is similar to what happens for the normalized driving force, Y_T. The swimming velocity is plotted in its real dimension, $\mu m/s$, to provide a better sense about the motion performance. Considering the achievable order of magnitude for swimming velocity $\sim O(10^2)\,\mu$m/s, it is proved that the proposed swimmer may travel its size in a second. Comparing with many types of artificial or natural living matter swimmers [6,7,19–25,105,106], the swimming velocity is satisfactory.

For the given example, the Reynolds number is estimated as, $\Re = \rho a V_s/\eta \sim O(10^{-2})$, which is in consistency with the assumption of low Reynolds number in the presented theories and reflection method.

From the design point of view, the optimal range of the frequency of operation and the aspect ratio, to get the maximum swimming velocity, are important. Figure 7 shows the optimal frequency of operation for selected aspect ratios

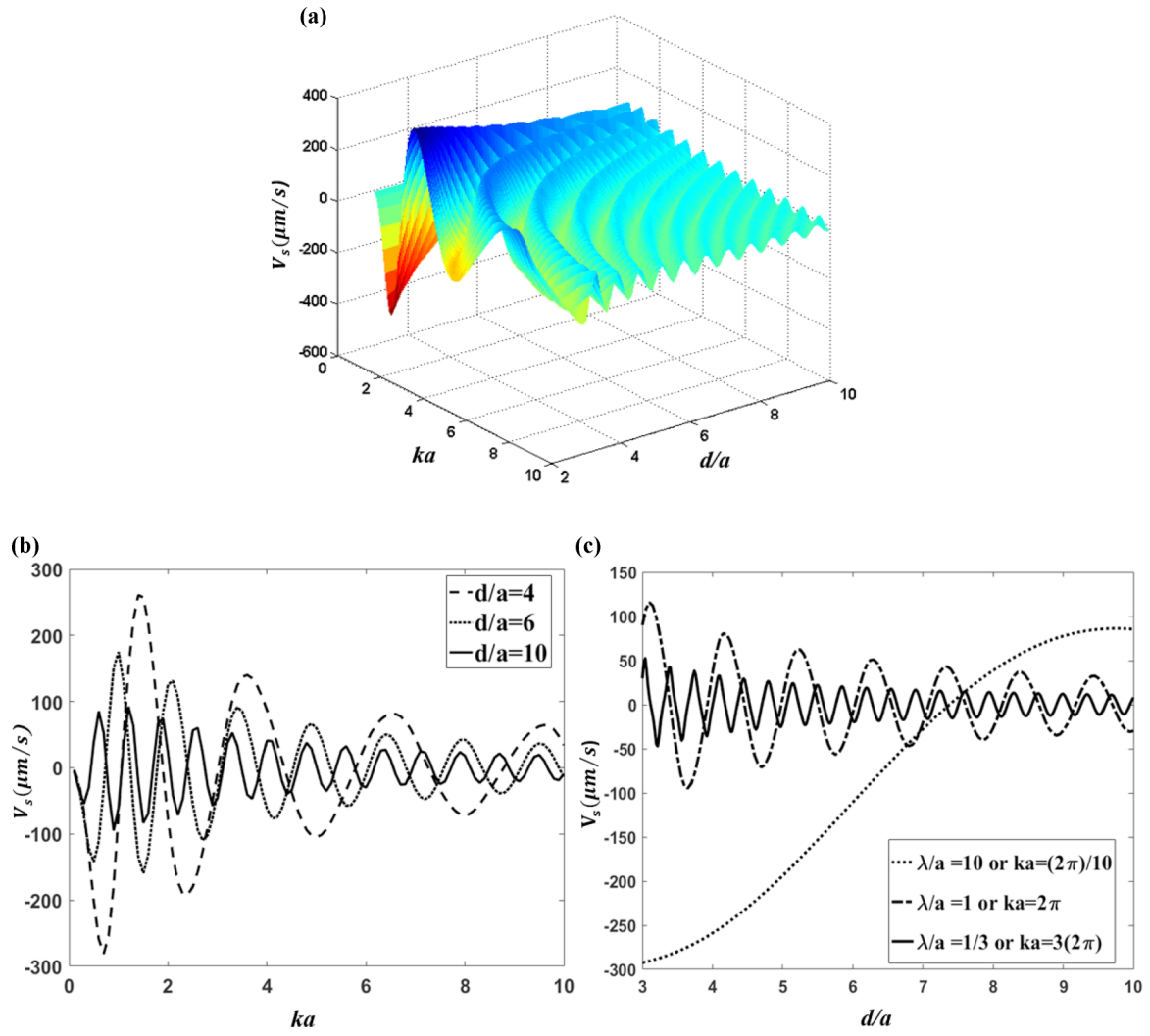

FIG. 6. (a) Three-dimensional (3D) plot of swimming velocity, V_s, as a function of nondimensional frequency, $0 < ka < 10$, and geometrical aspect ratio, $3 < d/a < 10$, corresponding to the maximum swimming state. (b) Some selected slices of 3D plot of V_s for selected aspect ratios, $d/a = 4,\ 6,\ 10$. (c) Some selected slices of 3D plot of V_s for three categories of wavelength to radius of spheres ratios as $\lambda/a = 10,\ 1,\ 1/3$ [i.e., $(2\pi)/10,\ 2\pi,\ 3(2\pi)$] corresponding to low, medium, and high wavelength to size ratios. (Configuration 1.)

in the range of, $3 \leqslant d/a \leqslant 10$. It is found that the optimal range of frequency lies within the range of $0.5 < ka < 1.5$, or the wavelength to size ratio of $4.2 < \lambda/a < 12.6$. For the case of our numerical example, the optimal range of operating frequency is $1.18\,\text{MHz} < \omega/2\pi < 3.53\,\text{MHz}$. Considering the practical considerations and the design procedures for construction of acoustic spherical radiators, the radially polarized piezoelectric coated with compatible materials (e.g., chemically resistivity and biocompatibility) is the best choice in which the required amplitude of radiation and frequency, is feasible by imposing appropriate and practicable AC voltages on the implemented electrodes [56,84,85,87,107].

The following paragraphs study the second configuration composed of a single acoustic radiating sphere and a cargo container, for the limited case of $d/a_1 = 4$.

Figures 8(a) and 8(b) compare the three approximation orders of swimming velocity, V_s, obtained from the reflection method, up to first, third, and fifth order of aspect ratio index, $O(a_1^{p_1} a_2^{p_2}/d^{p_1+p_2})$, as functions of nondimensional frequency, ka_1, and size ratio, a_2/a_1, respectively. In spite of configuration 1, as the frequency increases, the errors between the approximations increase. The same happens as the size ratio of container to radiating sphere, a_2/a_1, increases. In the worst state (i.e., $ka_1 = 10$ and $a_2/a_1 = 2$), the first-order approximation overestimate the swimming velocity up to 70%, while the error between the third and fifth orders of approximation does not exceed than 10%. It should be noted that all approximation in reflection method, keep the true patterns of variations. Therefore, by proper choosing of maximum required order of approximation, the general behavior of solution seems stable and robust; thus, there is no vital need to provide exact solutions to estimate the swimming velocity, in the first steps of design and feasibility studies.

Figure 9(a) illustrates the 3D pattern of swimming velocity of swimmer, V_s, as a function of nondimensional frequency of operation, $0 < ka_1 < 10$, and size ratio, $1 < a_2/a_1 < 2$. Figure 9(b) shows the top view of Fig. 9(a), in which the green regions are corresponding to negative velocities (i.e., leftward motion) and yellow regions indicate the positive values (i.e., rightward motion). Figure 9(c) depicts some selected 2D size

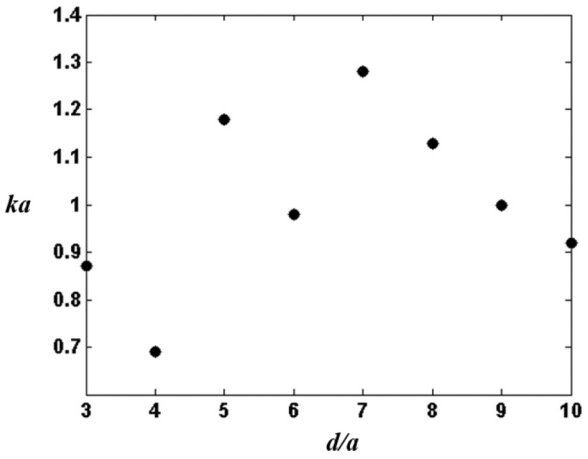

FIG. 7. The optimal frequency of operation, to achieve maximum swimming velocity, for selected aspect ratios in the range of $3 \leqslant d/a \leqslant 10$. (Configuration 1.)

ratio slices of Fig. 9(a) at $a_2/a_1 = 1$, $a_2/a_1 = 1.5$, $a_2/a_1 = 2$. Figure 9(d) depicts some selected 2D frequency slices of Fig. 9(a) at $ka_1 = 0.8$, $ka_1 = 2$, and $ka_1 = 10$.

The order of magnitude of the maximum swimming velocity is $\sim O(10^2)\,\mu$m/s. The maximum attainable swimming velocity is one-half of the case of configuration 1, $\approx 150\,\mu$m/s. The swimming velocity pattern shows an increasing trend with respect to size ratio, $1 < a_2/a_1 < 2$, up to one order of magnitude. It is not obvious since increasing the size of cargo-container or body 2, may lead to higher drag force. The observed behavior may be interpreted in the following manner. Without body 2, the symmetric monopole (breathing mode) radiation of radiating sphere induces just symmetric pressure and momentum fields in host medium and there is no reason for net motion. The existence of body 2 breaks the symmetry. The emerged asymmetric fluctuation in the induced acoustic field, leads to appearance and growth of nonlinear interaction terms in driving acoustic radiation force on the swimmer which has direct correlation to size ratio, a_2/a_1. In a sensible analogy, the body 2 plays the role of mainsail of the sailboat.

Another observed feature in Fig. 9(b) is the limited frequency bandwidth in which the leftward motion or negative values for swimming velocity is feasible. The order of magnitude of the negative swimming velocity is $\sim O(10^1)\,\mu$m/s. Figure 10(a) shows the occurrence frequency of maximum negative swimming velocity for selected aspect ratios. It is clear that for frequencies higher than a specified maximum for quantized size ratios, a_2/a_1, the swimming is just in rightward direction, or the swimming velocity takes positive values. Figure 10(b) shows the mentioned specified maximum frequencies for quantized selected size ratios. The obtained frequency ranges for our numerical example is $\sim O(10^0)$ MHz, which is practical and feasible.

Making comparison with the case of configuration 1, it may be concluded that the configuration 2 face with a serious challenge for directional maneuverability (i.e., directional maneuverability means both states of rightward and leftward motions along the desired direction can be achieved), due to this fact that the leftward motion is not achievable at all frequency ranges, but changing the frequency of radiation may overcome this problem.

Considering the probable fluctuations in the host medium which may cause deviation of the swimmer from its desired path which should swim along it, or in the case of any need for steering, both configurations 1 and 2 face to challenge. It may be resolved by following suggestions. Assume the configuration 1 and a desired path depicted in Fig. 11(a). Changing the state of swimmer to $\Delta\Phi = 180^\circ$ (i.e., zero net driving force) and switching on the external wave driver along the desired path and operating with the same frequency of radiating spheres (to avoid the multi-frequency field issues), due to asymmetry, it is expected that an external torque, normal to plane of motion (i.e., the plane composed of wave propagation direction and z axis) induces so that make the swimmer aligned on the desired path. Considering some approximations, an estimation of timescale required for alignment may be useful. Following Ref. [54], the time-averaged acoustic external radiation force exerted on a radiating sphere

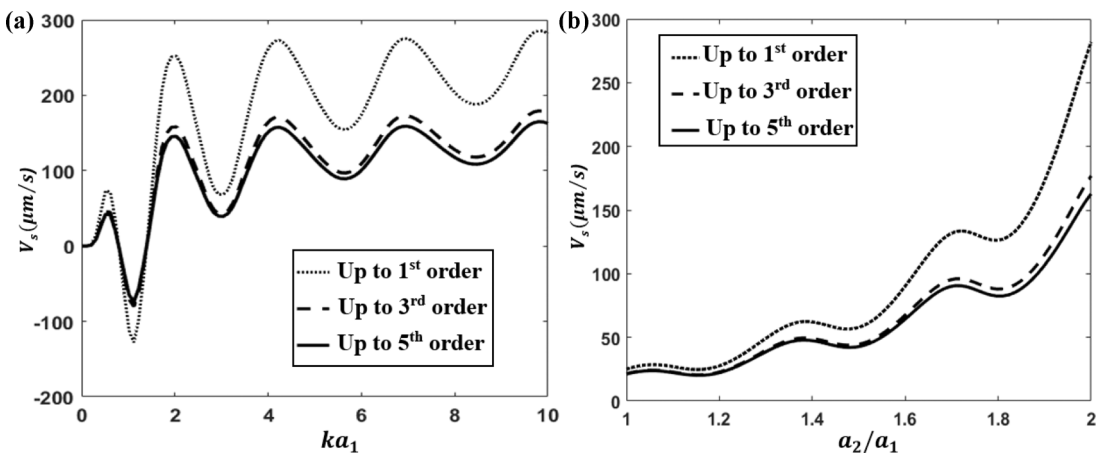

FIG. 8. The comparison between the three approximation orders of swimming velocity, V_s, obtained from the reflection method, up to first, third, and fifth order of aspect ratio index, $O(a_1^{p_1} a_2^{p_2}/d^{p_1+p_2})$, as functions of nondimensional frequency, ka_1, and size ratio, a_2/a_1. (Configuration 2.)

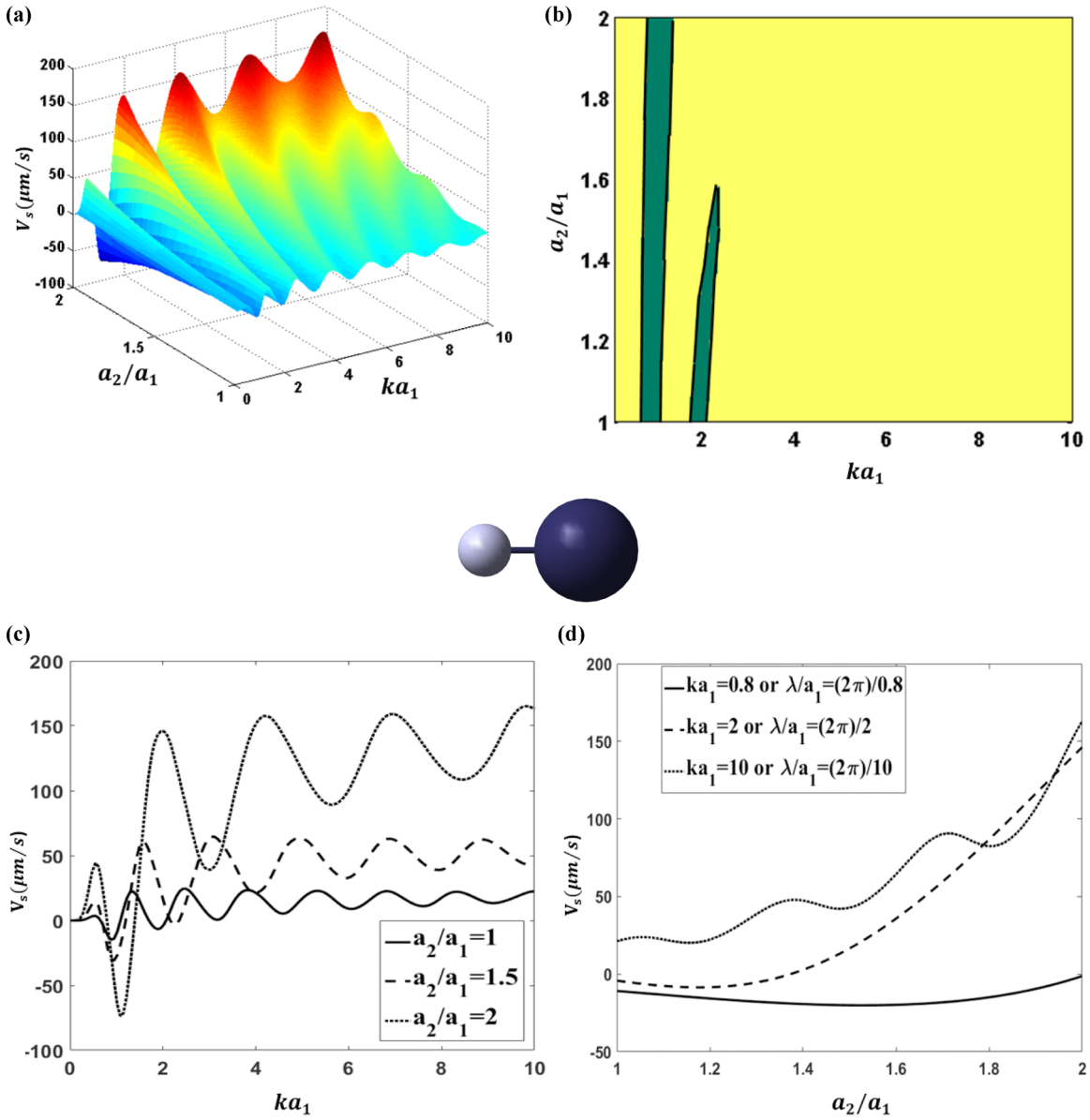

FIG. 9. (a) The 3D plot of swimming velocity of swimmer, V_s, in the case of configuration 2, as a function of nondimensional frequency of operation, $0 < ka_1 < 10$, and size ratio, $1 < a_2/a_1 < 2$. (b) The top view of 3D plot of swimming velocity, in which the green regions are corresponding to negative velocities (i.e., leftward motion) and yellow regions indicate the positive values (i.e., rightward motion). (c) Some selected slices of 3D plot of swimming velocity at $a_2/a_1 = 1$, $a_2/a_1 = 1.5$, $a_2/a_1 = 2$. (d) Some selected slices of 3D plot of swimming velocity at $ka_1 = 0.8$, $ka_1 = 2$ and $ka_1 = 10$. (Configuration 2.)

in its breathing mode, due to an incident plane wave field, is found as $\langle \boldsymbol{F} \rangle = \langle \boldsymbol{F} \rangle_0 + \langle \boldsymbol{F} \rangle_a \sin(2\pi Z/\lambda + \Delta\phi)$ where Z is the position coordinate along the wave-field propagation direction or desired direction, λ is the wave length of the radiated or incident wave fields, $\Delta\phi$ is the phase difference between the incident wave field and the radiator, $\langle \boldsymbol{F} \rangle_0$ is the acoustic radiation force on the spherical body in its passive state and $\langle \boldsymbol{F} \rangle_a$ is the amplitude of fluctuation of phase (position)-dependent radiation force term. Neglecting the acoustic radiation interaction between the two same-sized radiators, $\langle \boldsymbol{F} \rangle_0$ leads to translational motion of the device, but $\langle \boldsymbol{F} \rangle_a$ may lead to compensation of angular deviation, due to the possible resistant torque exerted upon the device. For the considered configuration 1, and the external forces due to the navigation wave field along the Z axis are $\langle \boldsymbol{F} \rangle_1 = \langle \boldsymbol{F} \rangle_0 + \langle \boldsymbol{F} \rangle_a \sin(2\pi Z_1/\lambda + \Delta\phi_1)$ and $\langle \boldsymbol{F} \rangle_2 = \langle \boldsymbol{F} \rangle_0 + \langle \boldsymbol{F} \rangle_a \sin(2\pi Z_2/\lambda + \Delta\phi_2)$, which lead to external torque as $\tau_e = [\langle \boldsymbol{F} \rangle_a d \sin(\varepsilon)/2][\sin(2\pi(Z_2 - d\cos(\varepsilon))/\lambda + \Delta\phi_1) - \sin(2\pi Z_2/\lambda + \Delta\phi_2)]$ where α is the deviation angle between the symmetry axis of swimmer and the desired path. For the case of configuration 1 which the radiators are out of phase (i.e., $\Delta\phi_1 = \Delta\phi_2 + \pi$) and for the limiting range of $d/\lambda \ll 1$, the external torque may be approximated as $\tau_e \approx -\langle \boldsymbol{F} \rangle_a d \sin(\varepsilon) \sin(2\pi Z_2/\lambda + \Delta\phi_2)$. The hydrodynamics resistant torque exerted upon the device, at low Reynolds number state, may be estimated as $\tau_h \approx -2\dot{\alpha}[8\pi\mu a^3 + 6\pi\mu a(d/2)^2]$ in which the first term is due to the spin and the second term is due to the trans-

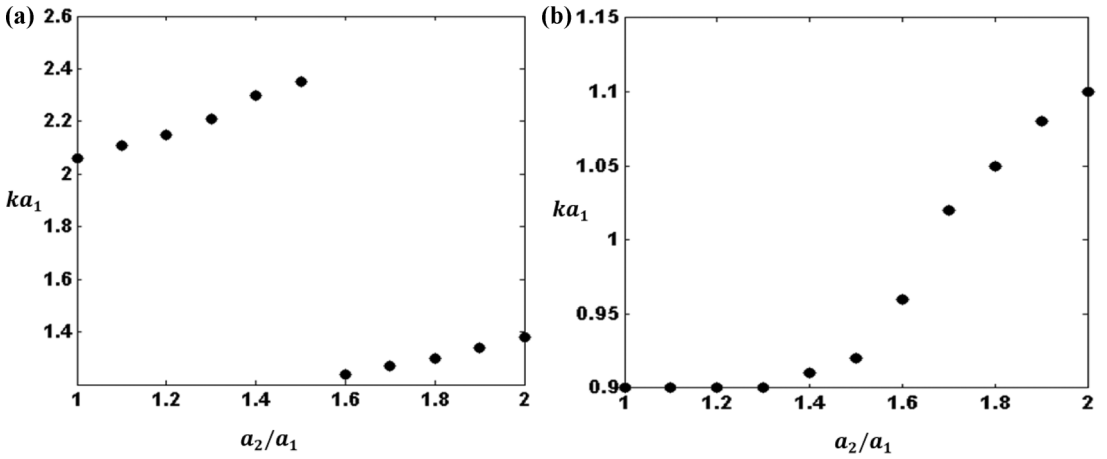

FIG. 10. (a) The frequency of radiation for which the maximum negative swimming velocity occurs for selected aspect ratios, in the case of configuration 2. (b) The specified maximum frequencies for which the negative swimming velocity or leftward motion is possible in the case of configuration 2, for selected size ratios. (Configuration 2.)

lational motion due to the rotation [93]. Considering the steady state condition and the torque balance, and assuming the stable state of the device, we find $\tau_h + \tau_a = 0$, which for small deviation angles leads to $\dot{\varepsilon}_{\max} \sim -\zeta\varepsilon$, where $\zeta \sim O(\langle \boldsymbol{F} \rangle_a d/\pi\mu a[16a^2 + 3d^2])$. The solution of the obtained variation rate of deviation angle, is $\varepsilon(t) = \varepsilon_0 e^{-\zeta t}$, where ε_0 is the maximum deviation angle before the action of navigation wave field. For the practical amplitudes of incident wave field as $P_0 = 10^4$ Pa, and following the analytical analysis of Ref. [54], we find $O(\langle \boldsymbol{F} \rangle_a) \sim O(\langle \boldsymbol{F} \rangle_0) \sim O(\pi a^2 P_0^2 Y/(2\rho c^2)) \sim O(10^{-9})\, N$ where $Y \sim O(1)$ is the nondimensional radiation force function. As an estimation for timescale of alignment, the minimum required timescale for alignment, t_a, with the assumed condition of $\varepsilon(t_a) = \varepsilon_0/100$, is calculated as $t_a = (-1/\zeta)\ln(\varepsilon(t_a)/\varepsilon_0) \sim O(10^{-1})\, s$. The obtained timescale is satisfactory since the translational motion of the device during this steering process, is estimated as $\approx V_s t_a \sim O(\langle \boldsymbol{F} \rangle_0 t_a/(12\pi\mu a)) \sim O(10^2)\, \mu$m. It should be noticed that the above estimation should be updated and modified considering the true hydrodynamics of the problem and the interaction terms due to the nonlinear superposition of the radiated, the scattered and the incident wave fields, nevertheless, as an approximation may help to have a practical sense. It is apparent that another state of zero driving force, $\Delta\Phi = 0^\circ$, is prone to another stable orientation, normal to the desired path, which is not desired. The emphasis on the state of zero net motion during the steering is to confine the unwanted translational motion of the swimmer and providing the possibility of pure rotational motion of swimmer; nevertheless, due to the possible unbalanced interaction of wave fields with radiating spheres, the unwanted translational motion during the rotational maneuvering is probable [54,55]. Clearly, the presented approach for steering is not optimal and should be enhanced in future. Also, the effects of acoustic radiation torque should be taken into account.

Following the same methodology, for the case of configuration 2, especially its asymmetric state, $a_2 \neq a_1$, the inherent geometrical asymmetry leads to induction of stabilizing torque as seen in Fig. 11(b). Therefore, the steering by using an external source is achievable.

IV. CONCLUSION

In conclusion, we have presented a novel self-propulsive swimming mechanism at low Reynolds number based on nonlinear effects associated with the acoustic radiation force phenomenon. The introduced microsized swimmer is composed of two linked spheres, acoustically radiating in their

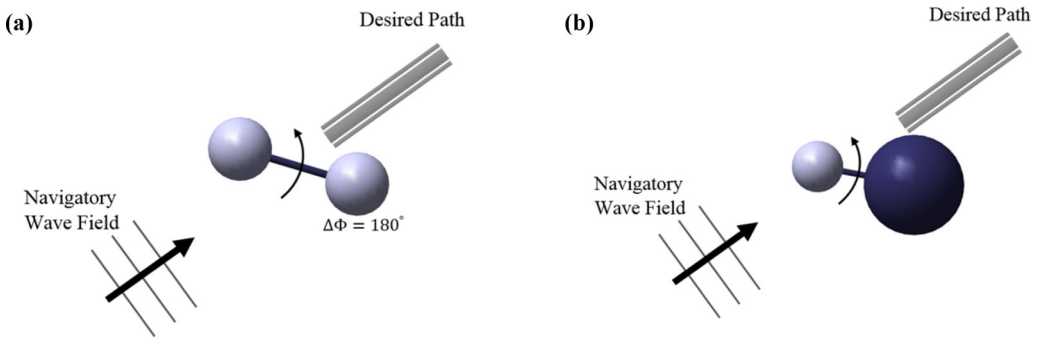

FIG. 11. (a) The schematic that shows the induced torque effect and the manipulability of the swimmer configuration 1, along the desired path, by an externally driven temporary acoustic wave field. (b) The schematic that shows the induced torque effect and the manipulability of swimmer configuration 2, along the desired path, by an externally driven temporary acoustic wave field.

breathing mode. Analytically, it is shown that the interaction of induced acoustic field with the spheres in nonlinear regime, leads to a net frequency dependent driving force, propelling the swimmer through the host medium. Decoupling the acoustic field from the hydrodynamics of the flow, the swimming velocity is estimated using the reflection method assuming nonslip boundary condition on the Stokes flow.

The driving force and swimming velocity are examined as functions of size ratios and radiating conditions (i.e., nondimensional frequency, possible phase difference between the radiators) for two different configurations. The first configuration is arranged by two same size radiating sphere which resembles as a double motorboat. It has been shown that the maximum swimming velocity is achieved in the phase differences of $\Delta\Phi = \pm 90^\circ$ and the directional steering is possible by shifting the phase difference as $\Delta\Phi = \mp 90^\circ$. The second configuration, presents the case of a single spherical radiator and a cargo container. The offered configuration may serve as a safe carrier considering the concerns and difficulties about the possible hazards of carrying agent, material, or drug, which may require special specifications. Surprisingly, it has been observed that the swimming velocity shows direct relation with the size of container due to what we call sail effect. The leftward motion of this single motor configuration is limited to specific bandwidth of frequencies. However, in both configurations, the achievable swimming velocity goes up to the order of swimmer length per second, which is acceptable comparing with other types of swimmers.

In the presented solutions, all simplification and assumptions may be supported by convincing justifications, but the presented theories may be developed by considering the coupling effects between the acoustic and hydrodynamics fields. In addition, modifications due to the viscosity effects of fluidic medium on the radiation force calculations may be implemented in future works.

In conclusion, the versatility, simplicity, feasibility, controllability, and satisfactory swimming performance of the proposed self-propulsive or self-motile swimmer could attract researchers to open an area of investigation toward the generation of acoustic-driven swimmers, carriers, delivery systems, mechanisms, robotics, manipulators, trappers, etc., and may advance the technology of micro- or molecular-sized machines.

[1] G. Iddan, G. Meron, A. Glukhovsky, and P. Swain, Nature **405**, 417 (2000).

[2] K. Ishiyama, M. Sendoh, A. Yamazaki, M. Inoue, and K. I. Arai, IEEE Trans. Magn. **37**, 2868 (2001).

[3] K. Ishiyama, M. Sendoh, A. Yamazaki, and K. Arai, Sens. Actuators A **91**, 141 (2001).

[4] G. Taylor, in *Proceedings of the Royal Society of London A: Mathematical, Physical and Engineering Sciences* (The Royal Society, London, 1951), Vol. 209, pp. 447–461.

[5] E. M. Purcell, Am. J. Phys. **45**, 3 (1977).

[6] E. M. Purcell, Proc. Natl. Acad. Sci. **94**, 11307 (1997).

[7] A. Najafi and R. Golestanian, Phys. Rev. E **69**, 062901 (2004).

[8] P. Lammert, J. Prost, and R. Bruinsma, J. Theor. Biol. **178**, 387 (1996).

[9] W. F. Paxton, K. C. Kistler, C. C. Olmeda, A. Sen, S. K. St. Angelo, Y. Cao, T. E. Mallouk, P. E. Lammert, and V. H. Crespi, J. Am. Chem. Soc. **126**, 13424 (2004).

[10] S. Fournier-Bidoz, A. C. Arsenault, I. Manners, and G. A. Ozin, Chem. Commun. **4**, 441 (2005).

[11] N. Mano and A. Heller, J. Am. Chem. Soc. **127**, 11574 (2005).

[12] G. Rückner and R. Kapral, Phys. Rev. Lett. **98**, 150603 (2007).

[13] J. R. Howse, R. A. L. Jones, A. J. Ryan, T. Gough, R. Vafabakhsh, and R. Golestanian, Phys. Rev. Lett. **99**, 048102 (2007).

[14] Y. Hong, N. M. K. Blackman, N. D. Kopp, A. Sen, and D. Velegol, Phys. Rev. Lett. **99**, 178103 (2007).

[15] B. Abécassis, C. Cottin-Bizonne, C. Ybert, A. Ajdari, and L. Bocquet, Nat. Mater. **7**, 785 (2008).

[16] R. Golestanian, T. Liverpool, and A. Ajdari, New J. Phys. **9**, 126 (2007).

[17] M. J. Mercier, A. M. Ardekani, M. R. Allshouse, B. Doyle, and T. Peacock, Phys. Rev. Lett. **112**, 204501 (2014).

[18] J. A. Cohen and R. Golestanian, Phys. Rev. Lett. **112**, 068302 (2014).

[19] W. F. Paxton, S. Sundararajan, T. E. Mallouk, and A. Sen, Angew. Chem. Int. Ed. **45**, 5420 (2006).

[20] R. Golestanian, T. B. Liverpool, and A. Ajdari, Phys. Rev. Lett. **94**, 220801 (2005).

[21] W. F. Paxton, A. Sen, and T. E. Mallouk, Chem. Eur. J. **11**, 6462 (2005).

[22] S. Ebbens, M.-H. Tu, J. R. Howse, and R. Golestanian, Phys. Rev. E **85**, 020401 (2012).

[23] M. Lighthill, Commun. Pure Appl. Math. **5**, 109 (1952).

[24] Z. Lin, J.-L. Thiffeault, and S. Childress, J. Fluid Mech. **669**, 167 (2011).

[25] S. Wang and A. Ardekani, Phys. Fluids **24**, 101902 (2012).

[26] G. Hancock, in *Proceedings of the Royal Society of London A: Mathematical, Physical and Engineering Sciences* (The Royal Society, London, 1953), Vol. 217, pp. 96–121.

[27] S. J. Lighthill, *Mathematical Biofluiddynamics* (SIAM, Philadelphia, 1975).

[28] R. E. Goldstein, T. R. Powers, and C. H. Wiggins, Phys. Rev. Lett. **80**, 5232 (1998).

[29] S. Camalet, F. Jülicher, and J. Prost, Phys. Rev. Lett. **82**, 1590 (1999).

[30] J. Blake, J. Fluid Mech. **46**, 199 (1971).

[31] A. Shapere and F. Wilczek, J. Fluid Mech. **198**, 557 (1989).

[32] A. Shapere and F. Wilczek, J. Fluid Mech. **198**, 587 (1989).

[33] H. A. Stone and A. D. T. Samuel, Phys. Rev. Lett. **77**, 4102 (1996).

[34] A. Ajdari and H. A. Stone, Phys. Fluids **11**, 1275 (1999).

[35] K. M. Ehlers, A. Samuel, H. C. Berg, and R. Montgomery, Proc. Natl. Acad. Sci. USA **93**, 8340 (1996).

[36] N. Phan-Thien, T. Tran-Cong, and M. Ramia, J. Fluid Mech. **184**, 533 (1987).

[37] J. Lighthill, in *The Centenary of a Paper on Slow Viscous Flow by the Physicist H. A. Lorentz* (Springer, Berlin, 1996), pp. 35–78.

[38] S. A. Koehler and T. R. Powers, Phys. Rev. Lett. **85**, 4827 (2000).
[39] V. A. Vladimirov, J. Fluid Mech. **717** (2013).
[40] D. Klotsa, K. A. Baldwin, R. J. A. Hill, R. M. Bowley, and M. R. Swift, Phys. Rev. Lett. **115**, 248102 (2015).
[41] R. Dijkink, J. Van Der Dennen, C. Ohl, and A. Prosperetti, J. Micromech. Microeng. **16**, 1653 (2006).
[42] D. Ahmed, M. Lu, A. Nourhani, P. E. Lammert, Z. Stratton, H. S. Muddana, V. H. Crespi, and T. J. Huang, Sci. Rep. **5**, 9744 (2015).
[43] H. Bruus, Lab Chip **12**, 1014 (2012).
[44] J. Wu, J. Acoust. Soc. Am. **89**, 2140 (1991).
[45] P. L. Marston, J. Acoust. Soc. Am. **120**, 3518 (2006).
[46] J. Lee and K. K. Shung, Ultrasound Med. Biol. **32**, 1575 (2006).
[47] J. Lee and K. K. Shung, J. Acoust. Soc. Am. **120**, 1084 (2006).
[48] J. Lee, K. Ha, and K. K. Shung, J. Acoust. Soc. Am. **117**, 3273 (2005).
[49] P. L. Marston and D. B. Thiessen, Ann. N.Y. Acad. Sci. **1027**, 414 (2004).
[50] P. L. Marston, J. Acoust. Soc. Am. **125**, 3539 (2009).
[51] S. Xu, C. Qiu, and Z. Liu, Europhys. Lett. **99**, 44003 (2012).
[52] Y. Li, C. Qiu, S. Xu, M. Ke, and Z. Liu, Sci. Rep. **5**, 13063 (2015).
[53] S. Zhang, C. Qiu, M. Wang, M. Ke, and Z. Liu, New J. Phys. **18**, 113034 (2016).
[54] M. Rajabi and A. Mojahed, Ultrasonics **83**, 146 (2018).
[55] M. Rajabi and A. Mojahed, J. Sound Vib. **383**, 265 (2016).
[56] M. Rajabi and A. Mojahed, Ann. Phys. **372**, 182 (2016).
[57] M. Rajabi and A. Mojahed, Acta Acust. Acust. **103**, 210 (2017).
[58] M. Wang, C. Qiu, S. Zhang, R. Han, M. Ke, and Z. Liu, Phys. Rev. E **96**, 052604 (2017).
[59] F. Mitri, J. Phys. A: Math. Theor. **42**, 245202 (2009).
[60] M. Azarpeyvand and M. Azarpeyvand, Ultrasound Med. Biol. **40**, 422 (2014).
[61] M. Azarpeyvand, M. A. Alibakhshi, and R. Self, IEEE Trans. Ultrason. Ferroelectr. Freq. Control **59**, (2012).
[62] F. Cai, Z. He, Z. Liu, L. Meng, X. Cheng, and H. Zheng, Appl. Phys. Lett. **99**, 253505 (2011).
[63] C. R. Courtney, C. E. Demore, H. Wu, A. Grinenko, P. D. Wilcox, S. Cochran, and B. W. Drinkwater, Appl. Phys. Lett. **104**, 154103 (2014).
[64] F. Li, F. Cai, Z. Liu, L. Meng, M. Qian, C. Wang, Q. Cheng, M. Qian, X. Liu, J. Wu *et al.*, Phys. Rev. Appl. **1**, 051001 (2014).
[65] Y. Yamakoshi and Y. Noguchi, Ultrasonics **36**, 873 (1998).
[66] Y. Choe, J. W. Kim, K. K. Shung, and E. S. Kim, Appl. Phys. Lett. **99**, 233704 (2011).
[67] Y. Liu and J. Hu, J. Appl. Phys. **106**, 034903 (2009).
[68] D. Foresti, N. Bjelobrk, M. Nabavi, and D. Poulikakos, J. Appl. Phys. **109**, 093503 (2011).
[69] V. Vandaele, P. Lambert, and A. Delchambre, Precis. Eng. **29**, 491 (2005).
[70] J. D. Adams and H. T. Soh, Appl. Phys. Lett. **97**, 064103 (2010).
[71] J. Whitehill, A. Neild, T. W. Ng, and M. Stokes, Appl. Phys. Lett. **96**, 053501 (2010).
[72] E. P. Mednikov, in *Acoustic Coagulation and Precipitation of Aerosols* (Consultants Bureau, Washington, DC, 1965).
[73] L. Rozenberg, *Physical Principles of Ultrasonic Technology* (Springer Science & Business Media, Berlin, 2013), Vol. 1.
[74] K. Yasuda, S.-i. Umemura, and K. Takeda, Jpn. J. Appl. Phys. **34**, 2715 (1995).
[75] C. E. Brennen, *Cavitation and Bubble Dynamics* (Cambridge University Press, Cambridge, 2013).
[76] T. Leighton, *The Acoustic Bubble* (Academic Press, 2012).
[77] L. A. Crum, R. A. Roy *et al.*, Phys. Today **47**, 22 (1994).
[78] X. Chen and R. E. Apfel, J. Acoust. Soc. Am. **99**, 713 (1996).
[79] A. Mojahed and M. Rajabi, Ultrasonics **86**, 1 (2018).
[80] O. B. Wilson, *Introduction to Theory and Design of Sonar Transducers*, Vol. 3 (Peninsula Publishing, Los Altos, CA, 1988).
[81] S. Snyder, N. Tanaka, and Y. Kikushima, J. Vibrat. Acoust. **117**, 311 (1995).
[82] A. Babaev and V. Savin, Int. Appl. Mech. **31**, 887 (1995).
[83] C. E. Ruckman and C. R. Fuller, J. Acoust. Soc. Am. **96**, 2817 (1994).
[84] A. Babaev and L. Dokuchaeva, Int. Appl. Mech. **38**, 477 (2002).
[85] C. Scandrett, J. Acoust. Soc. Am. **111**, 893 (2002).
[86] V. Savin and I. Morgun, Int. Appl. Mech. **43**, 238 (2007).
[87] M. Rajabi and A. Mojahed, Phys. Rev. E **96**, 043001 (2017).
[88] A. D. Pierce and R. T. Beyer, J. Acoust. Soc. Am. **87**, 1826 (1990).
[89] E. A. Ivanov, *Diffraction of Electromagnetic Waves on Two Bodies* (National Aeronautics and Space Administration, Springfield, VA, 1970), Vol. 597.
[90] A. Messiah, Appendix CI in Quant. Mech. **2**, 1054 (1962).
[91] T. Hasegawa and K. Yosioka, J. Acoust. Soc. Am. **46**, 1139 (1969).
[92] M. R. Maxey and J. J. Riley, Phys. Fluids **26**, 883 (1983).
[93] J. Happel and H. Brenner, *Low Reynolds Number Hydrodynamics: With Special Applications to Particulate Media* (Springer Science & Business Media, Berlin, 2012), Vol. 1.
[94] T. Hasegawa, Y. Hino, A. Annou, H. Noda, M. Kato, and N. Inoue, J. Acoust. Soc. Am. **93**, 154 (1993).
[95] M. Rajabi and M. Behzad, J. Sound Vib. **333**, 5746 (2014).
[96] M. Rajabi and M. Behzad, Ultrasonics **54**, 971 (2014).
[97] S. Wang, J. S. Allen, and A. M. Ardekani, Eur. J. Comput. Mech. **26**, 115 (2017).
[98] G. Gaunaurd, H. Huang, and H. Strifors, J. Acoust. Soc. Am. **98**, 495 (1995).
[99] H. C. Berg, *Random Walks in Biology* (Princeton University Press, Princeton, NJ, 1993).
[100] A. Doinikov, in *Proceedings of the Royal Society of London A: Mathematical, Physical and Engineering Sciences* (The Royal Society, London, 1994), Vol. 447, pp. 447–466.
[101] A. A. Doinikov, Phys. Rev. E **54**, 6297 (1996).
[102] A. A. Doinikov, J. Acoust. Soc. Am. **101**, 713 (1997).
[103] A. A. Doinikov, J. Acoust. Soc. Am. **101**, 722 (1997).
[104] A. A. Doinikov, J. Acoust. Soc. Am. **101**, 731 (1997).
[105] R. Dreyfus, J. Baudry, M. L. Roper, M. Fermigier, H. A. Stone, and J. Bibette, Nature **437**, 862 (2005).
[106] P. Tierno, R. Golestanian, I. Pagonabarraga, and F. Sagués, J. Phys. Chem. B **112**, 16525 (2008).
[107] V. Z. Parton and B. A. Kudryavtsev, *Electromagnetoelasticity: Piezoelectrics and Electrically Conductive Solids* (Taylor & Francis, London, 1988).